Transonic Shock Wave. Turbulent Boundary Layer Interaction on a Curved Surface

C. Nebbeling* and B. Koren**†

* *Faculty of Aerospace Engineering, Kluyverweg 1, Delft, the Netherlands*
** *Centre for Mathematics and Computer Science, Amsterdam, the Netherlands*

Delft Progr. Rep., 12 (1988) pp. 365-380
Received and Accepted: July 1988

This paper describes an experimental investigation of a transonic shock wave - turbulent boundary layer interaction in a curved test section, in which the flow has been computed by a 2-D Euler flow method. The test section has been designed such that the flow near the shock wave on the convex curved wall corresponds to that near the shock wave at the upper surface of a transonic airfoil. The ratio of the radius of curvature of the wind tunnel wall to the thickness of the undisturbed boundary layer is about 80, a mean value for modern transonic wings at cruising flight conditions. Mach number distributions near the shock wave obtained from holographic interferometry are compared with those from the Euler flow computations. Surface pressure measurements have been made at various upstream Mach numbers. In the interaction region, boundary layer measurements have been made at upstream Mach numbers of 1.15 and 1.37. The aim of the present experiment was to produce carefully the conditions prevailing along the upper surface of an airfoil in transonic flow. Attention is paid to the effects of surface curvature and static pressure rise downstream of the shock wave on boundary layer parameters and separation phenomena.

List of symbols

c	speed of sound
c_f	skin friction coefficient
H	shape factor ($=\delta^*/\theta$)
M	Mach number
p	pressure
r	recovery factor
R	radius of curvature (of streamline)
Re	Reynolds number
T	temperature
u	velocity component
u_τ	friction velocity
v	velocity component
x	horizontal coordinate
y	vertical coordinate
β_p	pressure gradient parameter ($=\frac{\theta}{u_e}\frac{du_e}{dx}$)
δ	boundary layer thickness
δ^*	boundary layer displacement thickness
θ	momentum thickness
ν	kinematic viscosity
ϕ	angle between streamline and x-axis

Superscript

i	incompressible

Subscripts

e	conditions at boundary layer edge
p	pitot
t	total
u	conditions just upstream of shock wave
δ	conditions related to boundary layer thickness

INTRODUCTION

The interaction between a shock wave and a turbulent boundary layer has been the subject of many investigations involving a variety of Mach numbers and boundary layer conditions. Often these investigations concerned boundary layers on a flat surface [1, 2, 3]. Since the work of BRADSHAW [4], it is known that streamline curvature diminishes the skin friction and enlarges the shape factor. However, the work of SCHOFIELD [3] merits attention by the application of a strong positive pressure gradient downstream of a shock wave - boundary layer interaction on a flat surface. A supersonic area downstream of the shock wave was found to occur already at $M_u = 1.41$, whereas without pressure gradient such a supersonic area occurs at $M_u \geqslant 1.44$.

An investigation by ALBER et al [5] in which surface curvature was considered, aimed at the determination of separation and attachment criteria for turbulent boundary layers. Since transonic shock wave - boundary layer interaction at free flight cruising conditions takes place in general at convex walls, the present investigation involves curvature effects in a flow in which a local transonic flow area is terminated by a curved normal shock wave. For this purpose a special curved test section was designed. The tests, which were made at $M_u = 1.15$ and $M_u = 1.37$, confirm the strong influence of curvature on the boundary layer parameters. Special attention has been given to the effects of pressure gradients downstream of the interaction. For both Mach numbers, the complete inviscid flow field in the wind tunnel has been computed by an Euler flow method [6]. The Euler code used allows designs better accomodating the experimentalist's requirements. Moreover, it yields additional information enabling a proper interpretation of complicated experimental results.

THE CURVED TEST SECTION

The experiments were performed in a curved two-dimensional test section of the ST15 blow-down wind tunnel at the Delft University of Technology. The test section, which is 150 mm wide and about 165 mm high, was designed such that the ratio of surface curvature and boundary layer thickness, $(R/\delta)_u$, corresponds to transonic free flight conditions. According to INGER [7] a value between 50 and 100 might fulfil this requirement. For the present design $(R/\delta)_u = 80$ has been retained. Since the expected boundary layer thickness near the shock wave was about 5.5 mm, the actual radius of curvature of the convex lower wall was chosen equal to 450 mm. The test section height followed from the condition that at $M_u = 1.45$, the Mach number at the (concave) upper wall of the test section should be 0.85 at a maximum [8]. This led to a test section height of about 165 mm. The final design is given in Fig. 1.

The need for side-wall boundary layer fences has been considered. However, preliminary measurements revealed a reasonable amount of two-dimensionality near the plane of symmetry without fences. Therefore, fences were omitted since they would have impeded the use of optical techniques. To ensure adiabatic wall conditions the convex curved nozzle block has been constructed of wood, clad with a 0.4 mm thick layer of phosphorus bronze, in which the surface pressure taps were drilled.

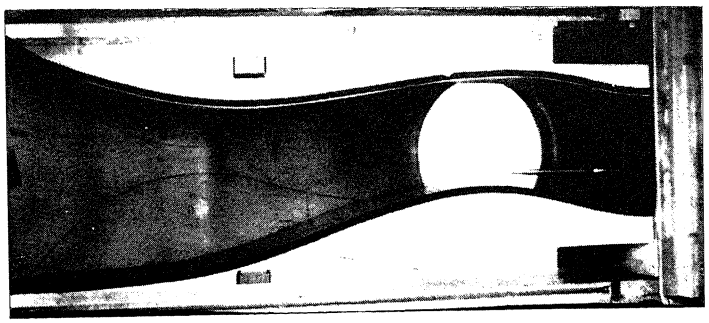

Fig. 1. Curved test section in opened wind tunnel.

EULER FLOW SOLUTIONS

Computational method

For a detailed description of discretization and solution method applied for the Euler equations, see [6, 9]. Briefly summarized, the Euler equations are discretized in their integral form, using the conservative formulation. The discretization method used is of upwind finite volume type, where the upwind scheme used is Osher's approximate Riemann solver [10]. To solve the nonlinear system of discretized equations, symmetric point Gauss-Seidel relaxation is used. This relaxation method is simple and robust but needs an acceleration. A suitable acceleration technique is found in nonlinear multigrid preceded by nested iteration.

Boundary conditions at in- and outlet

The inlet flow has been prescribed to be subsonic, so requiring three boundary conditions. Constant values $u = u_{inlet}$, $v = 0$, $c = c_{inlet}$ have been chosen. The choice of constant values was motivated by the fact that the inlet is flat and parallel.

The outlet flow is subsonic as well, so requiring one boundary condition. As the outlet part is non-flat and non-parallel, the outlet boundary condition cannot be as trivial as those at the inlet. The following possibility has been considered: $p = p(y)$, as solution of the equation of curvilinear motion

$$\frac{dp(y)}{dy} = \gamma \frac{p(y) M_{outlet}^2}{R(y)} \cos(\phi(y)). \tag{1}$$

For $1/R(y)$ and $\phi(y)$ linear distributions have been applied, such that they fitted the channel outlet. The subsonic value of M_{outlet} has been determined with the 1-D flow theory, assuming a sonic throat and a fully subsonic outflow. Using the corresponding value of p as value for p at the lower wall, an initial value problem was obtained, which has been solved by means of a Runge-Kutta-Merson method. Note that no measured data have been used for any boundary condition.

Numerical results

Computational results obtained for $M_u = 1.15$ and $M_u = 1.37$ are shown in Fig. 2 and 3. The white markers in Fig. 2 correspond to computed pressures at the lower surface, the black to measured pressures. In Fig. 3, a comparison is made between the computed Mach number distributions and distributions obtained in a non-intrusive way with an interferometer. A very satisfactory quantitative agreement is found away, of course, from the wall and shock wave. Yet, an important result as the pressure rise across the shock wave at the wall has been predicted very satisfactory as well. This indicates that the Euler code may be exploited for accurately designing experimental set-ups. Given an

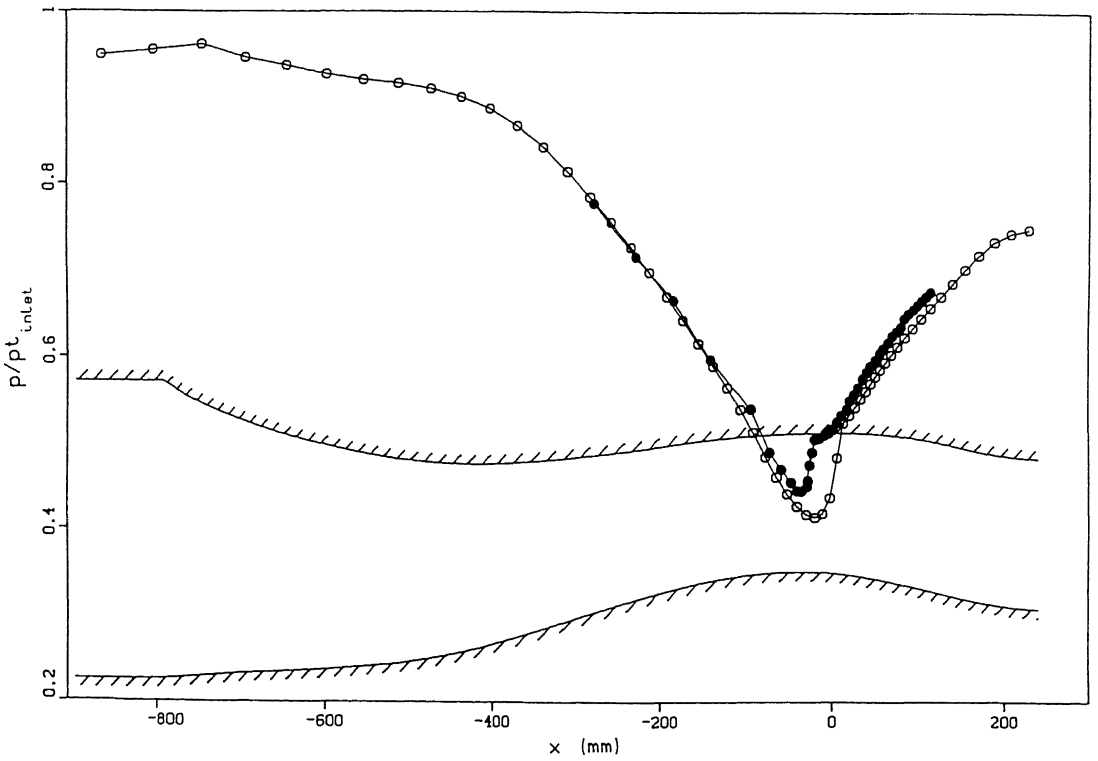

Fig. 2. Computed (O) and measured (●) surface pressure distributions.

a. At $M_u = 1.15$.

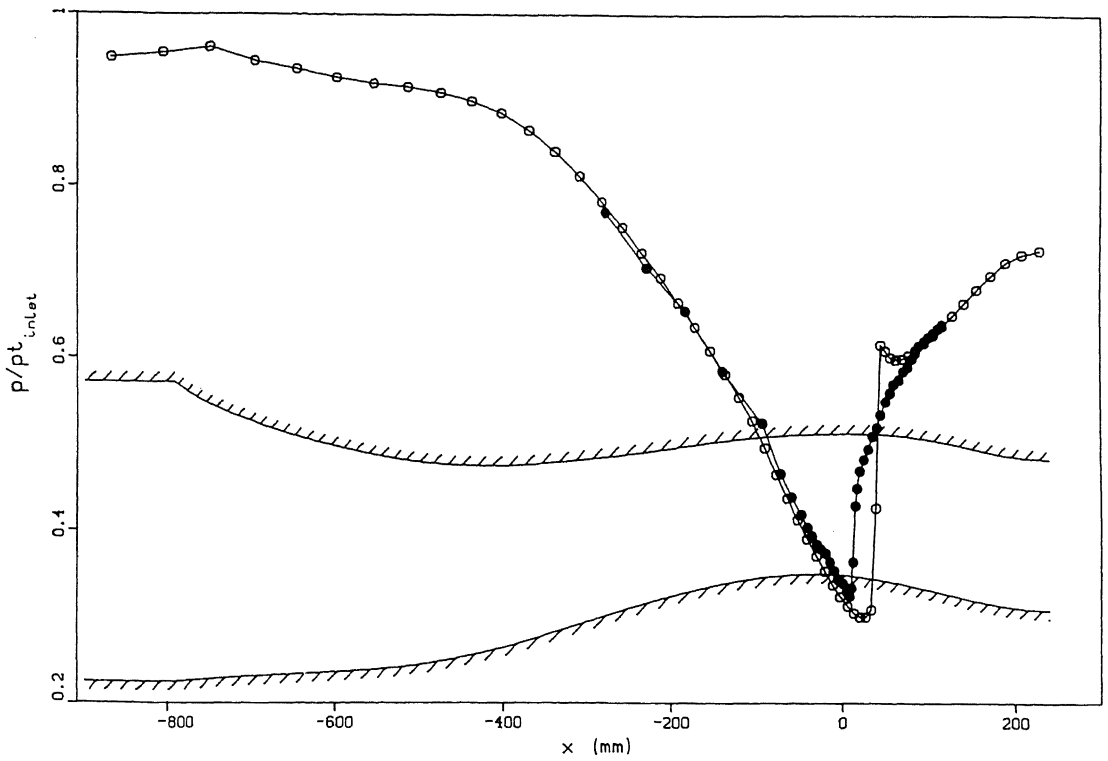

Fig. 2. **b. At $M_u = 1.37$.**

Euler code that has proved to be reliable, another possible exploitation is to use the differences between the computed and the experimental results for identifying simple viscous effects as well as more complicated viscous-inviscid phenomena. In these, the present Euler code has proved its reliability [11, 12, 13]. In the present paper, it shows that (i) the downstream supersonic expansion region and the shock bifurcation (at $M_u = 1.37$) are for a major part viscous-inviscid phenomena, and that (ii) the shock wave has been displaced slightly upstream by viscous effects.

Experimental techniques

The experiments were made at (i) $p_t = 1.65$ Bar, $M_u = 1.15$, and at (ii) $p_t = 1.8$ Bar, $M_u = 1.37$, both at $T_t \approx 270$ K. The specific Reynolds numbers were $Re = 2.7\ 10^7\ m^{-1}$ at $M_u = 1.15$ and $Re = 2.9\ 10^7\ m^{-1}$ at $M_u = 1.37$. Related to the measured boundary layer thickness just in front of the shock wave the Reynolds number is found to be $Re_\delta = 1.2\ 10^5$ for both flow conditions. The flow measurements were mainly restricted to pitot and static pressure probe traverses through the boundary layer, and to static surface pressure measurements. Most of the traverses were made with a computer controlled probe support downstream of the choke section. Pitot probes were used as Preston probes to provide the local skin friction coefficients. Schlieren and shadow pictures have been made to get an overall

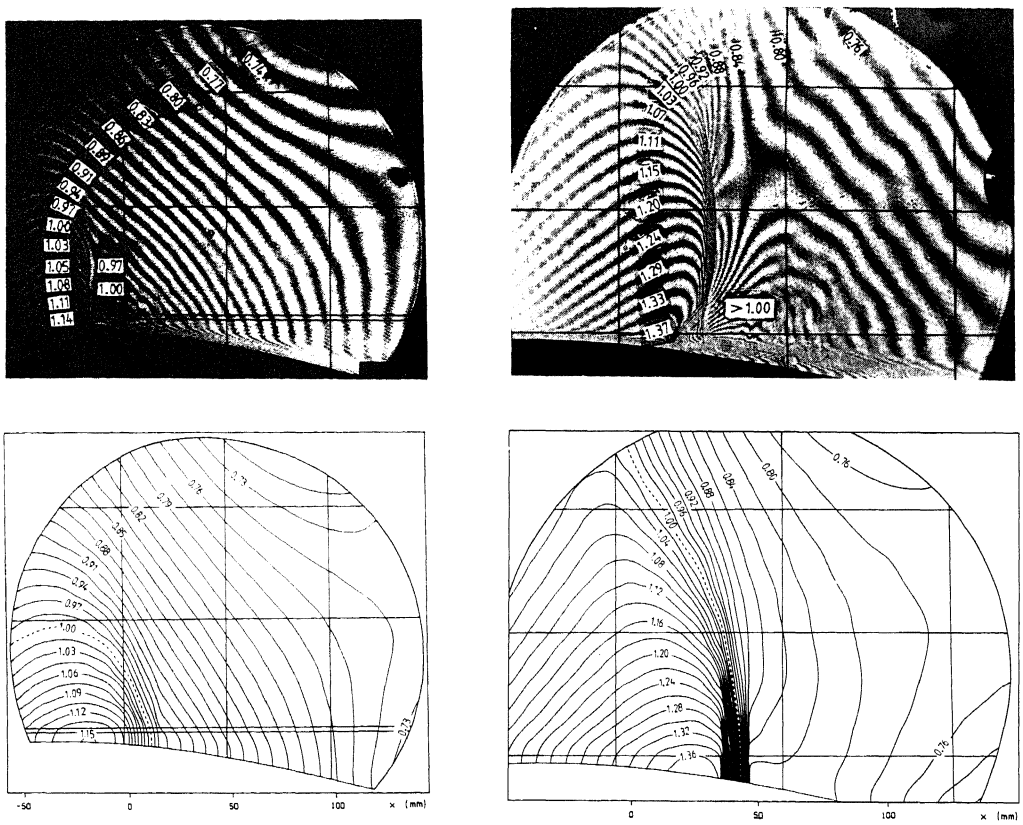

a. At $M_u = 1.15$. b. At $M_u = 137$.

Fig. 3. Computed and measured Mach number distributions.

impression of the flow field. Holographic interferometry allowed the determination of scalar quantities such as temperature and density. For details about the experimental techniques applied, see [14].

Boundary layer measurements

Surface pressure distribution

Prior to the boundary layer measurements, the flow downstream of the shock wave was examined for two-dimensionality in two different ways. First, the surface flow was visualized with a mixture of China clay, titanium-dioxide and oil. Thereafter, some pitot probe traverses were made at the plane of symmetry and at 25% of the tunnel width. Neither the surface flow visualization nor the pitot probe traverses show a severe lack of two-dimensionality at $M_u = 1.15$. At $M_u = 1.37$ three-dimensional effects were observed in both the pitot pressure distributions and the surface flow visuali-

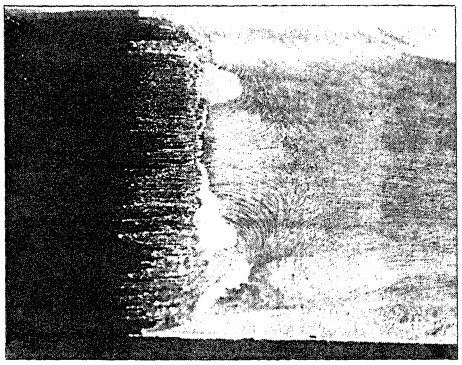

Fig. 4. Surface flow pattern at $M_u = 1.37$.

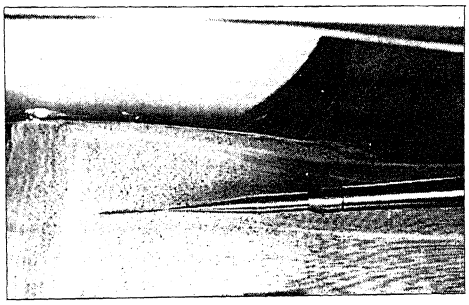

Fig. 5. Surface flow pattern with pressure probe touching the surface, at $M_u = 1.37$.

zations. For the latter upstream Mach number Fig. 4 shows the separation bubble downstream of the shock wave. The figure clearly shows that the centre part consists of a parallel surface flow, both inside and outside the separation region. Embarassing is Fig. 5 in which (for $M_u = 1.37$) a surface flow pattern is shown with the static pressure probe touching the wall surface and inducing a really two-dimensional surface flow. Considering the measurements, this phenomenon must be kept in mind.

Prior to the boundary layer measurements surface pressure distributions have been measured in the plane of symmetry with M_u ranging from 1.03 up to 1.37, including $M_u = 1.15$ (Fig. 6). These measurements at flow conditions not disturbed by probes provide a check of the accuracy of the static pressure probe measurements close to the wall. A common feature of most of the pressure distributions is that the steep pressure rise across the shock wave ends abruptly, and is followed by a less steep pressure increase or a plateau pressure, a phenomenon frequently observed at shock wave-boundary layer interactions. Peculiar in the present results is that the change in pressure increase occurs at a pressure level far below the local sonic pressure. In most reported investigations, this change in pressure gradient occurs near or above the sonic pressure [5, 15, 16]. A similar behaviour of the wall pressure distribution has been found only at very high Reynolds numbers [1, 17, 18]. The results of SCHOFIELD [3] seem to exclude the high downstream pressure gradient as the principal reason. At flat plate boundary layers PADOVA et al [18] also found abrupt changes in pressure gradient at pressure levels below the sonic wall pressure. These changes could be correlated to the bifurcation height of their shock wave. However, in the present experiments the shock wave was not bifurcated at the lower Mach numbers, and therefore surface curvature is expected to be the main cause. The much higher values of the plateau pressures at curved surfaces found in [19, 20], are probably caused by the non-smooth downstream joining of the convex hump and the flat wind tunnel wall in those experiments. This non-smooth joining agrees better with trailing edge conditions of an airfoil, however, concentration on curvature effects only, requires a smooth curvature profile downstream of the shock wave. In the case of flow separation at flat surfaces, a decrease in pressure gradient occurs

below the sonic pressure as well at higher Mach numbers, as measured by SEDDON [17]. Such a decrease is also found in the present measurements at the highest Mach number. However, this decrease is much larger at the lower Mach numbers, similar to the results of ALBER et al [5].

Normal static pressure distribution

Normal static pressure distributions have been measured up- and downstream of the shock wave at both $M_u = 1.15$ and $M_u = 1.37$. Traverses have been made (i) from 40 mm upstream of the shock wave up to 70 mm downstream at $M_u = 1.15$, and (ii) from 45 mm upstream to 60 mm downstream at $M_u = 1.37$. At $M_u = 1.37$, no differences in upstream static pressure distribution could be observed between the measurements in the plane of symmetry and those in a plane at 25% of the tunnel width. Downstream of the shock wave the differences are remarkable [14].

No static pressure traverses were made far upstream of the shock wave. Since the local flow curvature is small, the static pressure in the boundary layer was considered to be the measured surface pressure. In general the static pressure probe measurements near the surface agree fairly well with the measured

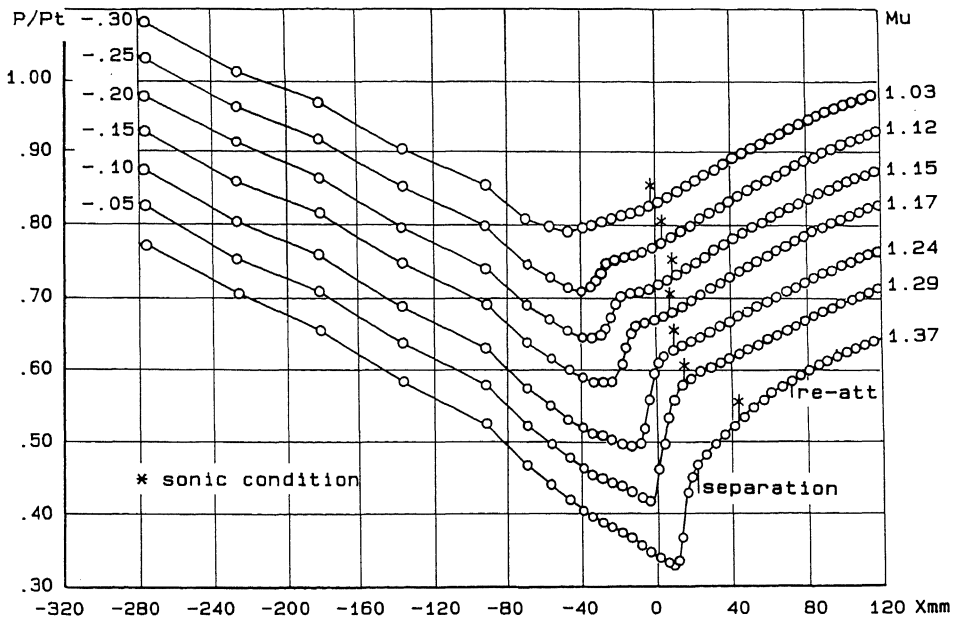

Fig. 6. Surface pressure distribution at different upstream Mach numbers.

surface pressures. Large differences occur only near the shock wave. Special attention must be paid to this at the data reduction to velocity profiles.

Mach number and velocity profiles

Pitot pressure traverses have been made for both upstream Mach numbers at 250 mm upstream of the shock wave and at locations corresponding to the static pressure traverses [14]. From these and the static pressure traverses, Mach number distributions in the boundary layer and in the inviscid flow region have been derived. Near the wall, a linear interpolation was used between the wall pressure - measured in the absence of the probes - and the nearest point of the normal static pressure traverse. However, close to the shock wave the probe static pressures are regarded as unreliable, considering the irregular shape of the pressure profile and the difference between the probe static pressures and the wall pressure. For these locations, the wall pressure has been taken as the static pressure in the boundary layer. A similar situation arises at $M_u = 1.37$ downstream of the shock wave where a region of separated flow is found. The static pressure probe seriously affects the separated flow, as shown by surface flow visualization, and the probe results close to the surface are questionable. The general shape of the static pressure profile as measured by the probe in this region shows decreasing static pressure towards the wall up to a distinct minimum value at some distance from the surface, followed by a static pressure increase to values well in excess of the wall pressure [14]. Such a pressure distribution is most unlikely and has to be ascribed to probe interaction. Therefore, the local wall pressure has been taken as the static pressure from the surface up to the distance where the measured probe pressure exceeds the wall pressure. Velocity profiles were calculated using the Crocco relation with $r = 0.89$ [14]. The velocity profiles are given in Fig. 7.

Skin friction distribution and flow separation

The skin friction distributions have been determined from Preston probe measurements as well as from Clauser plots. As far as the Preston probe measurements are concerned, the calibrations of PATEL [22] have been applied, corrected for compressibility effects by means of the reference temperature hypothesis. Since the compressibility corrections of ALLEN [23] led to more consistent results than those of SIGALLA [24], preference was given to Allen's functions. >From the Clauser plots the skin friction distributions were determined graphically for each measured velocity profile and corrected for compressibility using the Winter and Gaudet correction $c_f^i = c_f \sqrt{1+0.2M_e^2}$. The results from Preston probe measurements and Clauser plots are given in Fig. 8 for both $M_u = 1.15$ and $M_u = 1.37$. In general the skin friction values obtained from Patel's equations exceed those from the Clauser plots. This difference might be attributed to a difference in allowance for compressibility. For $M_u = 1.15$ the skin friction decreases about 30% near the shock wave followed by a slight recovery, after which a continuous reduction by the adverse pressure gradient starts without leading

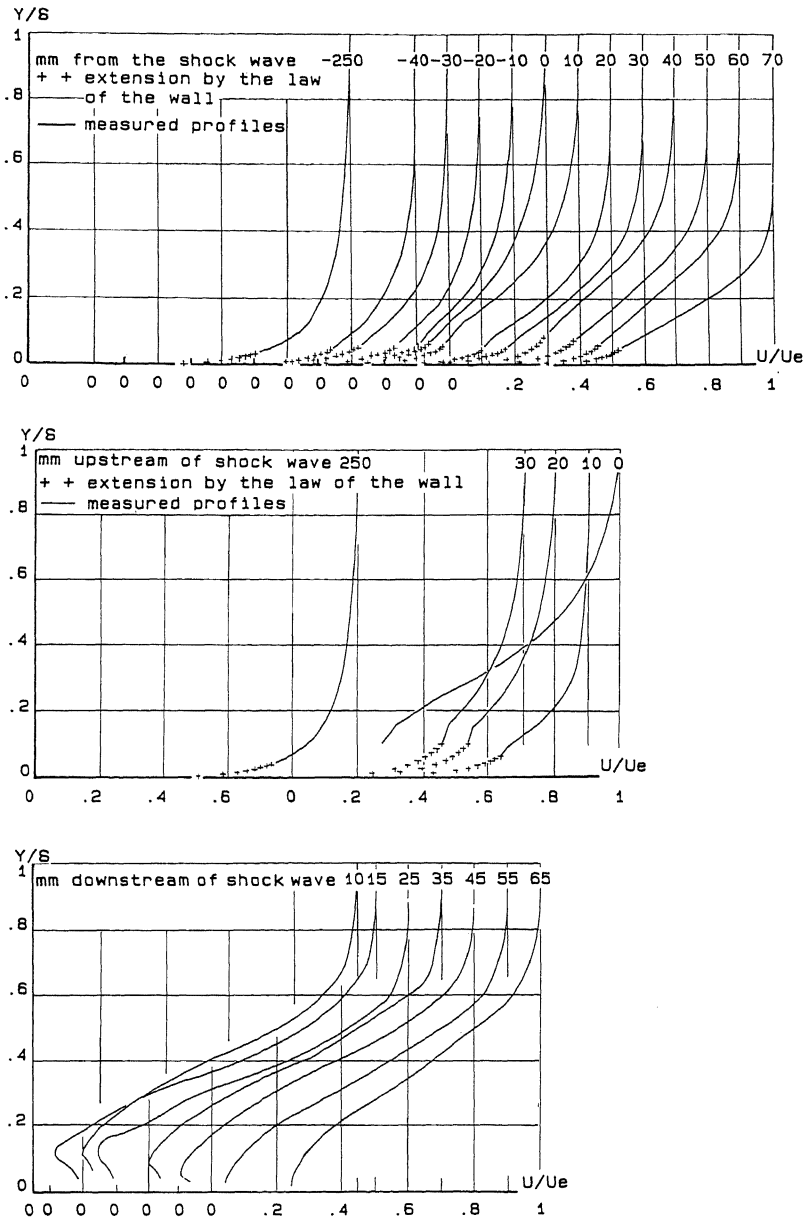

Fig. 7. Velocity profiles.

a. At $M_u = 1.15$.

b1. Upstream of shock wave, at $M_u = 1.37$.

b2. Downstream of shock wave, at $M_u = 1.37$.

however to a flow separation in the considered region. For $M_u = 1.37$ the skin friction distribution in downstream direction is quite different. Near the shock wave a steep reduction to a "zero" value occurs. This value persists for about 50 mm after which a gradual increase in the skin friction occurs. The location of the point where the skin friction starts to rise again cannot be determined with certainty due to the slight differences in c_f obtained by both methods. It may be argued that the Clauser plot method is open to doubt in this region as a well-developed turbulent boundary layer cannot be expected just downstream of the re-attachment. An extrapolation of the last three data points obtained by Preston probe measurements suggests a re-attachment point 46 mm downstream of the separation point, a value which seems compatible with the Clauser plot results. However, the oil flow visualization technique indicates a shorter separation length not exceeding 39 mm. Here again it must be remembered that the structure of the separated zone is significantly affected as soon as the pressure probe touches the surface, as shown by the oil flow patterns. This might explain why all measured skin friction values in the separated region are positive, independent of the method used.

Separation and re-attachment

Criteria for separation and re-attachment in transonic flow have been studied by ALBER et al [5]. These investigations yielded a description of shock- and pressure-induced separation of turbulent boundary layers. In agreement with [5], in the present investigation the shock-induced separation at $M_u = 1.37$ was observed at the maximum value of β_p (Fig. 9), but at re-attachment the value of β_p was only 0.0035, which is lower than the value given by ALBER et al.

It is pointed out that although the experimental set-up used by Alber et al resembles the set-up of the present experiment, an obvious difference is found in the wall contour downstream of the shock wave. In Alber's experiments the shock wave was located near an inflexion point in the surface and re-attachment of the flow occurred on the concave or flat surface downstream of this point. In the present experiment, re-attachment occurred on the continuing convex wall. This might be the cause of the difference in β_p at the re-attachment point, the more so as for both experiments the pressure gradient in the separated region is about 1.2 Bar/m.

Boundary layer thickness and integral parameters

To determine the boundary layer integral parameters the regular turbulent boundary layer profiles are extrapolated to the surface by means of the law of the wall in the compressible form of WINTER and GAUDET [21]:

$$\frac{u}{u_\tau^i} = 6.05 \log \frac{y u_\tau^i}{\nu_e} + 4.05 \qquad (2)$$

The incompressible friction velocity u_τ^i has been obtained by using the measured velocity nearest to the surface. Because of the severe shock-induced change of the regular turbulent boundary layer profile at $M_u = 1.37$, no extrapolations have been applied downstream of this shock wave.

Fig. 8. Wall shear stress distribution.

a. At $M_u = 1.15$.

b. At $M_u = 1.37$.

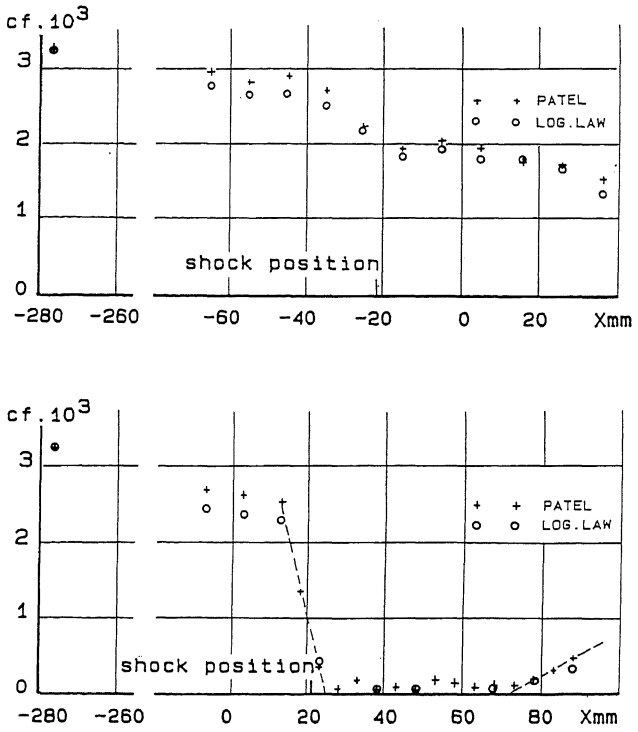

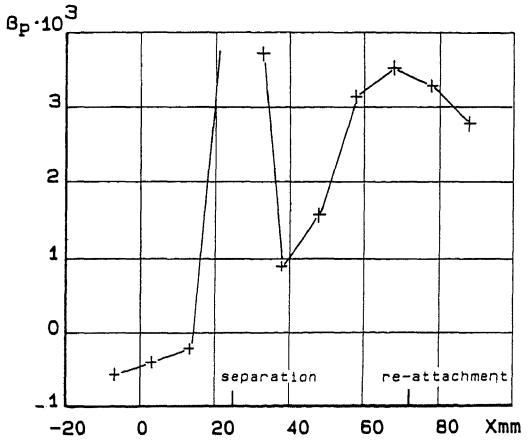

Fig. 9. Pressure gradient parameter distribution.

The boundary layer thickness δ, the integral parameters δ^* and θ, and the shape factor H are given in Fig. 10. The Reynolds numbers related to the shock positions are: $Re = 2.0\ 10^7$ respectively $2.3\ 10^7$. Because of the small difference in the main flow Reynolds numbers, the difference in boundary layer thickness must be imputed to differences in upstream pressure gradients. For $M_u = 1.37$ a substantial growth of the boundary layer occurs downstream of the shock wave. For $M_u = 1.15$ the boundary layer thickness seems to be little affected by the shock wave compared to the effect of the downstream pressure gradient. >From Fig. 10b and 10c it appears that the displacement thickness δ^* and the momentum thickness θ are affected immediately by the shock wave, even at the lower upstream Mach number. It is interesting to compare the results obtained at $M_u = 1.37$ with the results of Kooi and of Schofield. Kooi's measurements were made on a flat plate without pressure gradient at $M_u = 1.4$ and $Re = 2\ 10^7$ based on shock position. Schofield's experiments at $M_u = 1.41$ and $Re = 3.7\ 10^6$ were also made on a flat surface but with a strong adverse pressure gradient downstream of the shock. In the present results, the displacement thickness increases at $M_u = 1.37$ to about 8 times the upstream value, far in excess of the factor 4.5 in Kooi's experiment but in agreement with the factor 8.5 found by Schofield. This suggests that the difference with Kooi's value is due to the adverse pressure gradient rather than to the surface curvature.

The momentum thickness θ increases in the present experiment at $M_u = 1.37$ by a factor 2.5 through the shock wave and by a factor 3.8 up to the re-attachment point. This may be compared with the factor 3.2 reached far downstream in Kooi's experiment without downstream pressure gradient. At $M_u = 1.15$ the growth factor for the momentum thickness is about 1.4 which is rather high compared to the results of GADD [16].

The shape factor $H = \delta^*/\theta$ measured in the interaction region corresponds with results of Kooi, Schofield and Seddon at strong interactions. In a region of increasing shape factor, separation of the boundary layer is generally found where H reaches the value of 2.6. This is confirmed by the present investigation; no influence of the surface curvature or of the adverse pressure gradient on the shape factor at separation was observed. However, downstream of the flow separation H increases to a maximum value of 4.9, being much higher than the maximum value of 3.5 measured by Kooi. Based on numerical computations Inger obtained indications of an increase of the shape factor owing to surface curvature and a downstream adverse pressure gradient. In the present results H decreases within a rather short distance to a value which approaches the undisturbed upstream value. At a non-curved surface and with an adverse pressure gradient similar to that of the present measurements, Schofield has measured at $M_u = 1.41$ a maximum value of $H = 10.2$, the Reynolds number related to the shock position being $3.7\ 10^6$, i.e. 5 times less than in the present measurements. This implies a major effect of the adverse pressure gradient and in particular of the Reynolds number on the shape factor downstream of the shock wave.

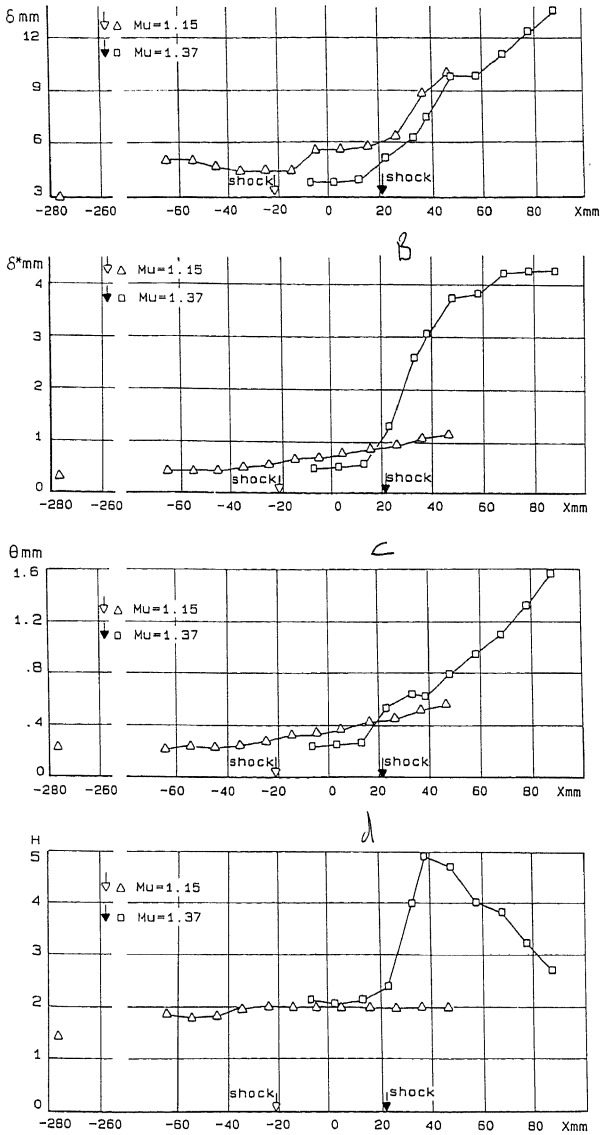

Fig. 10. Distributions of boundary layer thickness and integral parameters.

a. Boundary layer thickness.

b. Boundary layer displacement thickness.

c. Momentum thickness.

d. Shape factor.

CONCLUSIONS

The interaction between a shock wave and a turbulent boundary layer has been investigated at the convex wall of a blow-down wind tunnel with a curved test section. The Mach numbers just upstream of the shock wave were 1.15 and 1.37. At both Mach numbers a supersonic region downstream of the shock wave has been measured. The absence of such a supersonic region in the Euler flow computations suggests a dominant attribution of viscous effects in the flow field.

Surface curvature and an adverse pressure gradient downstream of the shock wave increase the growth of the boundary layer displacement thickness and the shape factor downstream of the shock wave in comparison to a corresponding flow structure at a flat plate and without adverse pressure gradient downstream of the shock wave.

Comparison with literature leads to the conclusion that the adverse pressure gradient downstream of the shock wave dominates the effects of surface curvature on the boundary layer. A successful comparison has been hampered however by the differences between the various test facilities.

No increase of the separation length has been measured with respect to experiments at non-curved surfaces.

The separation criterion of Alber et al agrees with the present findings. Re-attachment however, was found at a pressure gradient parameter $\beta_p = 0.0035$ instead of $\beta_p = 0.0065$ as given by Albert et al.

The usefulness of a reliable Euler code in research on viscous-inviscid interactions may be twofold. It may be used (i) as a tool for designing (and re-designing) an experimental set-up, and (ii) as a tool for understanding complicated experimental results. Given the recent availability of very reliable (and very efficient) Euler codes, this use might become of paramount importance in near-future research.

ACKNOWLEDGEMENT

The authors would like to thank J.G. Schepers for his contribution to the investigations.

REFERENCES

1. R.J. VIDAL, C.E. WITTLIFF, P.A. CATLIN and B.H. SHEEN, 1973. "Reynolds Number Effects on the Shock Wave-Turbulent Boundary Layer Interaction at Transonic Speeds", *AIAA-73-661.*
2. J.W. KOOI, 1975. "Experiments on Shock Wave-Boundary Layer Interaction", *AGARD CP-168.*
3. W.H. SCHOFIELD, 1983. "Interaction of a Turbulent Boundary Layer with a Normal Shock Followed by an Adverse Pressure Gradient", Defense Science and Technology Organisation, Aeronautical Research Laboratories, Melbourne, *Mechanical Engineering Report 161.*
4. P. BRADSHAW, 1973. "Effects of Streamline Curvature on Turbulent Flow", *Agardograph 169.*
5. I.E. ALBER, J.W. BACON, B.S. MASSON, and D.J. COLLINS, 1971. "An Experimental Investigation of Turbulent Transonic Viscous-Inviscid Interactions", *AIAA-71-565.*
6. B. KOREN, 1986. "Euler Flow Solutions for Transonic Shock Wave - Boundary Layer Interaction", to appear in *Int. J. for Num. Meth. in Fluids.*
7. G.R. INGER, 1981. "Transonic Shock-Turbulent Boundary Layer Interaction and Incipient Separation on Curved Surfaces", *AIAA-81-1244.*
8. C. NEBBELING and W.J. BANNINK, 1984. "A Curved Test Section for Research on Transonic Shock Wave-Boundary Layer Interaction", Delft University of Technology, *Report LR-414.*

9. P.W. HEMKER and S.P. SPEKREIJSE, 1986. "Multiple Grid and Osher's Scheme for the Efficient Solution of the Steady Euler Equations", *Appl. Num. Math. 2,* pp. 475-493.
10. S. OSHER and F. SOLOMON, 1982. "Upwind-Difference Schemes for Hyperbolic Systems of Conservation Laws", *Math. Comp. 38,* pp. 339-374.
11. P.W. HEMKER and B. KOREN, 1986. "A Non-linear Multigrid Method for the Steady Euler Equations", *Proceedings of the GAMM-Workshop on the Numerical Solution of Compressible Euler Flows,* Rocquencourt, Vieweg, Braunschweig.
12. B. KOREN, 1987. "Defect Correction and Multigrid for an Efficient and Accurate Computation of Airfoil Flows", to appear in *J. Comp. Phys.*
13. B. KOREN and S.P. SPEKREIJSE, 1987. "An Efficient Solution Method for the Steady Euler Equations", *Proceedings of the Third Copper Mountain Conference on Multigrid Methods,* Copper Mountain, Marcel Dekker, New York.
14. C. NEBBELING and B. KOREN, 1987. "An Experimental - Computational Investigation of Transonic Shock Wave - Turbulent Boundary Layer Interaction in a Curved Test Section", Centre for Mathematics and Computer Science, Amsterdam, *Report NM-R8716.*
15. J. ACKERET, F. FELDMANN, and N. ROTT, 1946. "Untersuchungen an Verdichtsstössen und Grenzschichten in Schnell Bewegten Gasen", Institut für Aerodynamik, ETH Zürich, *Bericht No.10.*
16. G.E. GADD, 1961. "Interactions between Normal Shock Waves and Turbulent Boundary Layers", *ARC R&M 3262.*
17. J. SEDDON, 1967. "The Flow produced by Interaction of a Turbulent Boundary Layer with a Normal Shock Wave of Strength sufficient to cause Separation", *ARC R&M 3502.*
18. C. PADOVA, T.J. FALK and C.E. WITTLIFF, 1980. "Experimental Investigation of Similitude Parameters governing Transonic Shock-Boundary Layer Interaction", *AIAA-80-0158.*
19. J. DÉLERY, 1978. "Analyse du Décollement résultant d'une Interaction Choc-Couche Limite Turbulente en Transonique", *Recherche Aerospatiale 6,* pp. 305-320.
20. X. LIU, and L.C. SQUIRE, 1985. "The Shock Wave-Turbulent Boundary Layer Interaction on a Curved Surface at Transonic Speed", *Proceedings of IUTAM Symposium,* Palaiseau, Springer, Berlin.
21. K.G. WINTER and L. GAUDET, 1970. "Turbulent Boundary Layer Studies at Mach Numbers between 0.2 and 2.8", *RAE TR 70251.*
22. V.C. PATEL, 1965. "Calibration of the Preston Tube and Limitations on its Use in Pressure Gradients", *J.F.M. 23,* pp. 185-208.
23. J.M. ALLEN, 1973. "Evaluation of Compressible Flow Preston Tube Calibrations", *NASA TN D-7190.*
24. A. SIGALLA, 1965. "Calibration of Preston Tubes in Supersonic Flow", *AIAA Journal, Vol. 3, No. 8,* pp. 1531.